Low-temperature cooling behavior of single-domain magnetite: Forcing of the crystallographic axes and interactions

Correction published 31 August 2006

Low-temperature cooling behavior of single-domain magnetite: Forcing of the crystallographic axes and interactions

Adrian R. Muxworthy[1,2] and Wyn Williams[2]

Received 18 January 2006; revised 6 April 2006; accepted 12 April 2006; published 18 July 2006.

[1] Low-temperature cycling (LTC) of magnetic remanences carried by rocks has become a standard technique in paleomagnetism, rock magnetism, and environmental magnetism as a means of identifying mineralogy and grain size. LTC usually involves measuring low-temperature thermomagnetic curves on cooling through crystallographic transitions, such as magnetite's Verwey transition. Historically, it has been assumed that remanence carried by single-domain (SD) magnetite grains is not affected by cooling through the cubic/monoclinic Verwey transition, whereas larger multidomain (MD) magnetite grains partially demagnetize. However, it has been recently pointed out that the shape anisotropy even for an infinitely long cylinder is approximately 3 times smaller than the monoclinic magnetocrystalline anisotropy along the hardest axis, i.e., SD remanences are not impervious to LTC. Using a micromagnetic algorithm we simulate LTC curves for assemblages of effectively elongated SD magnetite grains and consider the contribution of magnetostatic interactions. Initially, we assume that relationship between the cubic and monoclinic symmetry is chosen randomly; however, there are key experimental features, which this model does not explain. A new "controlled switching" model is developed; the orientation of the low-temperature monoclinic axes are not chosen randomly, but instead are controlled by the direction of the magnetic moment on cooling through the Verwey transition. This new model correctly predicts experimentally observed low-temperature trends that the "random" model does not. We therefore propose a new model for the mechanism controlling the behavior of SD grains at the Verwey transition and show that the low-temperature behavior of SD and MD grains can yield ambiguously similar behavior.

Citation: Muxworthy, A. R., and W. Williams (2006), Low-temperature cooling behavior of single-domain magnetite: Forcing of the crystallographic axes and interactions, *J. Geophys. Res.*, *111*, B07103, doi:10.1029/2006JB004298.

1. Introduction

[2] Low-temperature magnetic measurements have become increasingly popular as a means of identifying magnetic minerals, many of which display magnetic anomalies associated with various types of physical transitions. Because of the presence of magnetite in many natural systems, its distinctive Verwey transition, T_V, ($\sim$125 K) is of great interest and is commonly used as a method of identifying magnetite's presence [*Nagata et al.*, 1964]. At the Verwey transition many magnetic, electronic and crystallographic properties change, in particular the crystallographic cubic symmetry changes to monoclinic. This change in symmetry strongly affects the magnetocrystalline anisotropy, which not only changes shape (Figure 1), but in addition is an order of a magnitude greater in intensity than the cubic phase magnetocrystalline anisotropy at room temperature [*Bickford et al.*, 1957; *Abe et al.*, 1976].

[3] In multidomain (MD) magnetite this sharp change in the anisotropy directly influences a wide range of common magnetic properties, e.g., on cooling through T_V the coercive force increases and the susceptibility decreases [*Kronmüller et al.*, 1974; *Argyle and Dunlop*, 1990; *Özdemir et al.*, 2002]. Similarly, on either heating or cooling through T_V, the change in anisotropy causes demagnetization of saturation isothermal remanence (SIRM) induced in a MD grain [*Özdemir and Dunlop*, 1999].

[4] In contrast, it has been assumed that single domain (SD) grains are relatively unaffected by the Verwey transition. This assumption was based primarily on low-temperature demagnetization (LTD) memory ratios $\sim$1, where the memory ratio (MR) is the ratio of the magnetization at 300 K after cycling to $<T_V$ divided by the initial remanence. It was argued that MR $\sim$ 1 because most SD grains are controlled by the shape anisotropy at all temperatures, however, *Carter-Stiglitz et al.* [2002, 2004] pointed out that the maximum shape anisotropy (for an infinitely long cylinder) is approximately 3 times smaller than the monoclinic magnetocrystalline anisotropy along the hardest axis.

[1]Institute of Earth Science, University of Edinburgh, Edinburgh, UK.
[2]Department of Earth Science and Engineering, Imperial College, London, UK.

0148-0227/06/2006JB004298$09.00

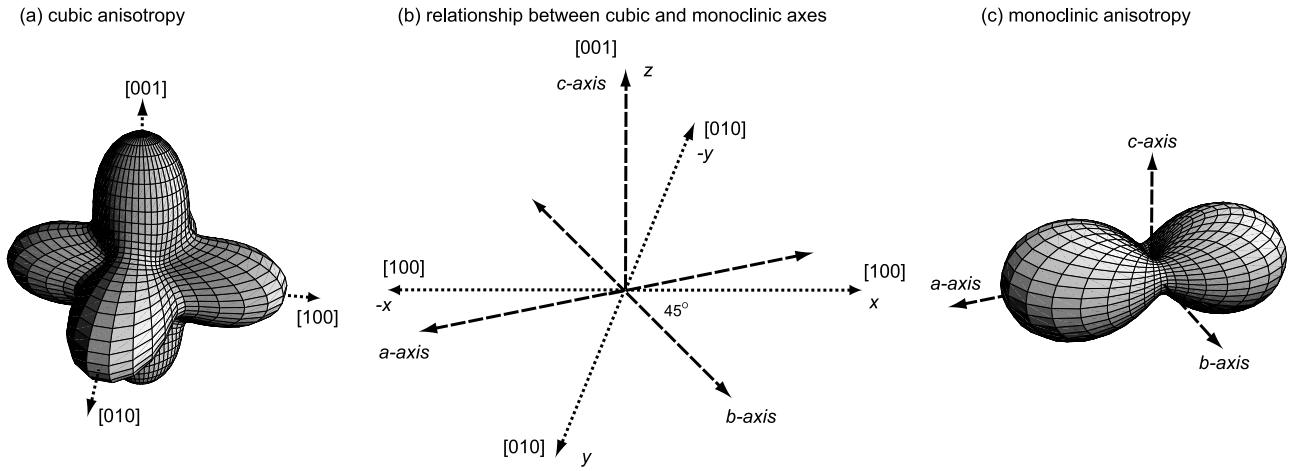

Figure 1. (a) Shape of the negative-cubic magnetocrystalline anisotropy field in magnetite, i.e., temperature >130 K, (b) schematic depicting the relationship between the high-temperature cubic crystallographic axis and the low-temperature monoclinic axis, and (c) the shape of the monoclinic anisotropy field in magnetite i.e., temperature < 120 K. The easy directions in both Figures 1a and 1c correspond to minimums in the field, i.e., the $\langle 111 \rangle$ directions in Figure 1a and the *c* axis in Figure 1c. The two anisotropies are not drawn on a relative scale; the maximum intensity of the monoclinic anisotropy field is ~25 greater.

That is, the magnetization of every SD grain will to a certain degree be affected on cooling below T_V.

[5] *Carter-Stiglitz et al.* [2004] modeled LTC curves for SIRMs induced in a assemblages of elongated, randomly orientated, noninteracting SD grains with varying uniaxial anisotropies defined in terms of q, where q is the ratio of the long axis to the short axis. They considered values of q between 1 (sphere, cube) and as $q \rightarrow \infty$ (infinitively long cylinder). In their model they assumed that during zero-field cooling (ZFC), the low-temperature phase orientation is chosen randomly with respect to the cubic anisotropy above T_V, i.e., the *c* axis aligns with one of the cube edges (Figure 1). In their model this gives rise to reversible behavior, i.e., MR ~ 1, with a large decrease in magnetization at T_V; the size of the decrease at T_V decreasing with increasing q (Figure 2).

[6] Their model did not include cubic magnetocrystalline anisotropy for temperatures greater than T_V. For large values of q this omission is not significant, however, for values of $q \leq 1.15$, the cubic magnetocrystalline anisotropy becomes increasingly important [*Geshev et al.*, 1998]. Because of this omission, near-equidimensional SD magnetite grains will behave differently to their model predictions, in particularly with respect to reversibility and predicted magnetic memory ratios. In addition to having a higher initial SIRM/M_S value, where M_S is the saturation magnetization, randomly orientated grains with random elongations of $q \leq 1.15$, are highly unlikely to display reversible behavior on cooling/warming through T_V (Figure 2). This is because on cooling through T_V the magnetic moments will realign to give a net demagnetization, but on warming back through T_V, the magnetic moments of near-equidimensional grains will have an eightfold (cubic) choice as to their new preferred direction rather than the twofold choice for uniaxial shape anisotropy. It is highly unlikely for assemblages of noninteracting grains that magnetic moments would all rotate back to their original positions, i.e., MR < 1.

[7] In addition, their model fails to predict certain key features that are commonly observed experimentally. For example, consider Figure 3 redrawn from *Özdemir et al.* [2002], which shows the LTC curves for near-cubic synthetic SD magnetite. On cycling through the T_V the magnetization is seen to partially reversibly increase, rather than decrease. To be consistent with previous studies [e.g., *Muxworthy et al.*, 2003a], we will refer to this anomalous jump on cooling through T_V as Δ_J, where Δ_J is the size of the anomalous jump normalized by the initial SIRM at 300 K (Figure 2). For Figure 3, Δ_J is positive. The model of *Carter-Stiglitz et al.* [2004] does not accommodate $\Delta_J > 0$.

[8] In this paper we investigate LTC curves for SD grains using a numerical micromagnetic approach. In the model developed in this paper we include several key features excluded from earlier models: first, we include magneto-

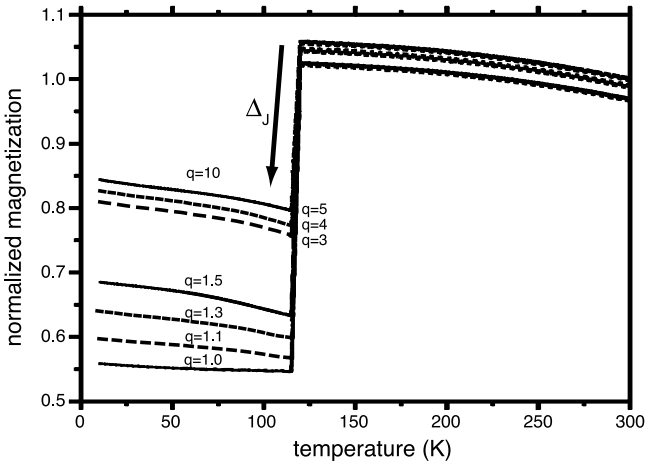

Figure 2. SIRM LTC simulations for assemblages of noninteracting SD grains with differing elongation factors q. Redrawn after *Carter-Stiglitz et al.* [2004]. Δ_J is also depicted.

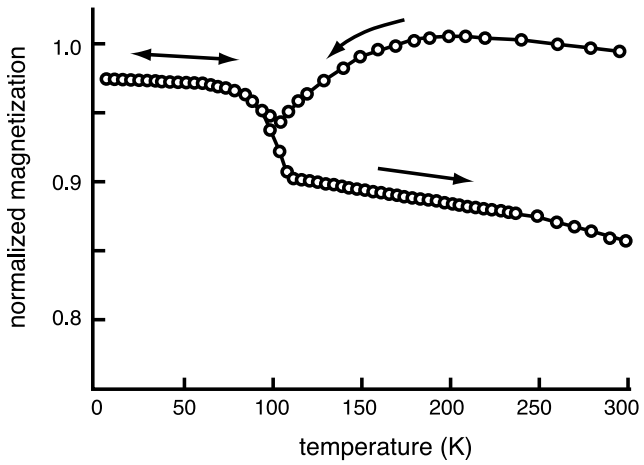

Figure 3. Experimental SIRM LTC curve for a synthetic magnetite sample of mean grain size 37 ± 15 nm (redrawn from *Özdemir et al.* [2002], copyright 2002, with permission from Elsevier).

crystalline anisotropy in the cubic phase above T_V in addition to a uniaxial anisotropy. Second, we consider the role of intergrain magnetostatic interactions on LTC. Third, we test the assumption made in earlier models that on zero-field cooling (ZFC) through T_V the low-temperature monoclinic *c* axis aligns randomly with one of the cubic axes (Figure 1); in this paper we consider in addition to the random alignment a second "controlled" alignment hypothesis.

2. Controlled Alignment Hypothesis

[9] The controlled alignment hypothesis assumes that the direction of the magnetic moment influences the choice of orientation of the monoclinic *c* axis (easy axis) at T_V. This hypothesis is driven by the idea that for any rotation of a magnetic moment there will be an associated energy barrier. If we temporally ignore other sources, which may influence the orientation of the *c* axis, then on cooling an SIRM (Figure 4a) through T_V, rather than randomly aligning with a cubic axis (Figure 4b), the *c* axis will align along the cubic axis closest to the magnetic moment (Figure 4c), that is the magnetic moment controls the direction of the *c* axis orientation. This hypothesis is not unreasonable as it is documented that in the presence of relatively small magnetic fields (field cooling, FC) of the same order as the coercivity, i.e., ~30–80 mT, that the *c* axis aligns with the direction of the field [*Carvallo and Muxworthy*, 2006]. The difference in this hypothesis is that for each grain the *c* axis aligns with direction of the remanence of each individual grain. That is, the resultant distribution of *c* axis orientations is partially ordered, rather than fully ordered as in the high-field FC case. The degree of ordering will increase with remanence value, so that an SIRM will have a greater degree of order than, say, a thermoremanence.

3. A Numerical Model for SD Low-Temperature Behavior

3.1. Micromagnetic Algorithm

[10] In this study we have implemented a combination micromagnetic algorithm [*Muxworthy and Williams*, 2004, 2005]. The approach combines both a minimum energy conjugate-gradient (CG) algorithm [e.g., *Williams and Dunlop*, 1989] and a dynamic algorithm which follows the torque of a magnetic moment according to the Landau-Lifshitz-Gilbert (LLG) equation [e.g., *Suess et al.*, 2002]. The reasoning behind this approach is that the dynamic algorithm gives the more rigorous solution since the magnetization between stable states must follow a physically reasonable path dictated by the LLG equation of motion; however, it is relatively slow compared to the CG method. In this combination algorithm, we use the CG algorithm to rapidly generate an initial guess for the magnetic structure, which is then put into the dynamic solver. This increases the efficiency of the algorithm by roughly an order of magnitude compared to the dynamic solver alone. We used a finitely damped solver detailed by *Brown et al.* [1989]. The combined method is more robust than the CG method alone, as it minimizes the torque on each discretized magnetic moment compared to the CG method, which only minimizes the total energy. The dynamic solver produces lower energy states than the CG algorithm alone. We use fast Fourier transforms (FFT) to calculate the demagnetizing energy, which allows the high resolution needed to examine arrays of interacting grains.

[11] In the model each grain is represented by a simple cube, that is, each cube represents the averaged magnetization direction of many hundreds of atomic magnetic dipole moments, or simply each cube is an ideal SD grain. The orientation of the magnetic moment of each grain can vary. The grain assemblage structure is initially calculated with the CG algorithm by minimizing the total magnetic energy, which is the sum of magnetostatic energy and the anisotropy E_A [*Brown*, 1963].

[12] E_A consisted of a cubic magnetocrystalline anisotropy above T_V and the monoclinic magnetocrystalline anisotropy below T_V in addition to a uniaxial anisotropy related to *q*. Details of the implementation of the crystallographic anisotropies and their temperature dependence have been described previously [*Muxworthy and Williams*, 1999]. Variations in the low-temperature crystallographic axes were taken from *Bickford et al.* [1957] and *Abe et al.* [1976]. These two data sets were chosen in favor over more recent data because they contain the most complete data sets with the highest number of temperature steps; the values correspond well with other published data. In the original study [*Muxworthy and Williams*, 1999] and this study, we omit the higher-order terms from the monoclinic magnetocrystalline anisotropy for two reasons. First, our model is a first-order approximation. Second, quick analytical calculations show that at all angles the terms selected to represent the monoclinic anisotropy dominate the other higher-order terms for two reasons: first, the absolute size of the intensity of the omitted terms is significantly smaller, and second, the higher-order terms are related to the directional cosines to the fourth power and not as in the lower-order terms, the second.

[13] In order to maintain the computational efficiencies of the FFT used in the algorithm, when generating the uniaxial anisotropy, rather than varying the shape of the particles we added an additional energy term of the form $E_A = K_U \sin^2\theta$, where θ is the angle between the elongation axis and the magnetization and K_U is a parameter related to the

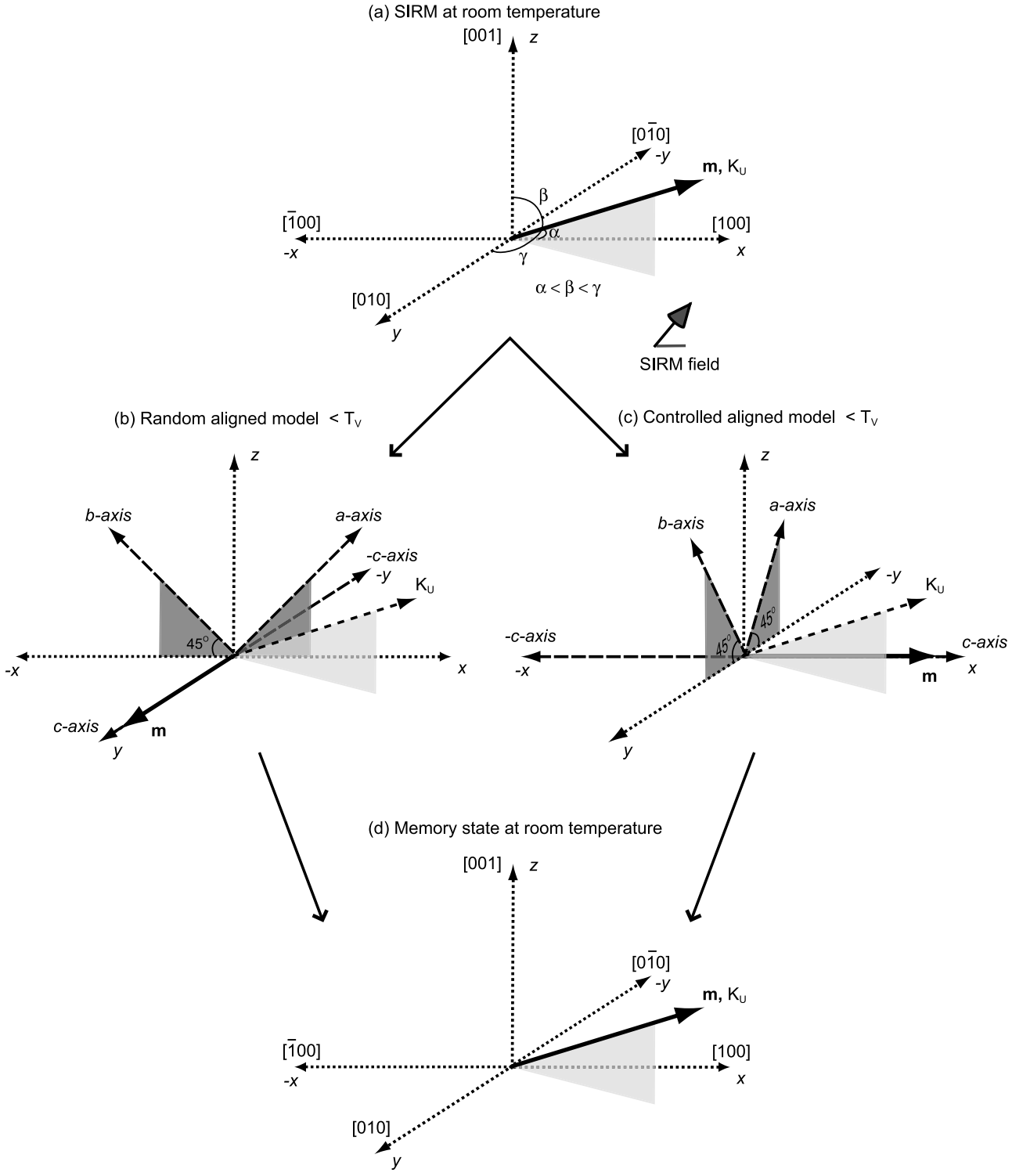

Figure 4. Schematic cartoon of the LTC SIRM behavior of a moment controlled by a uniaxial anisotropy (K_U) at room temperature for both the RA and CA models. This cartoon is for a noninteracting system. After the removal of a saturating field the magnetic moment will align with the nearest easy uniaxial axis, which is orientated at angles α, β, and γ with respect to the crystallographic axes (Figure 4a). From the same initial starting state (Figure 4a), the RA model switching behavior is shown in Figure 4b and for the CA model in Figure 4c. The resultant final state at room temperature after LTC is identical (Figure 4d). In CA model the moment switches to the closest ⟨100⟩ on passing through T_V. In the RA model the *c* axis is randomly chosen; that is, this schematic shows only one of six possible orientations of the monoclinic crystallography.

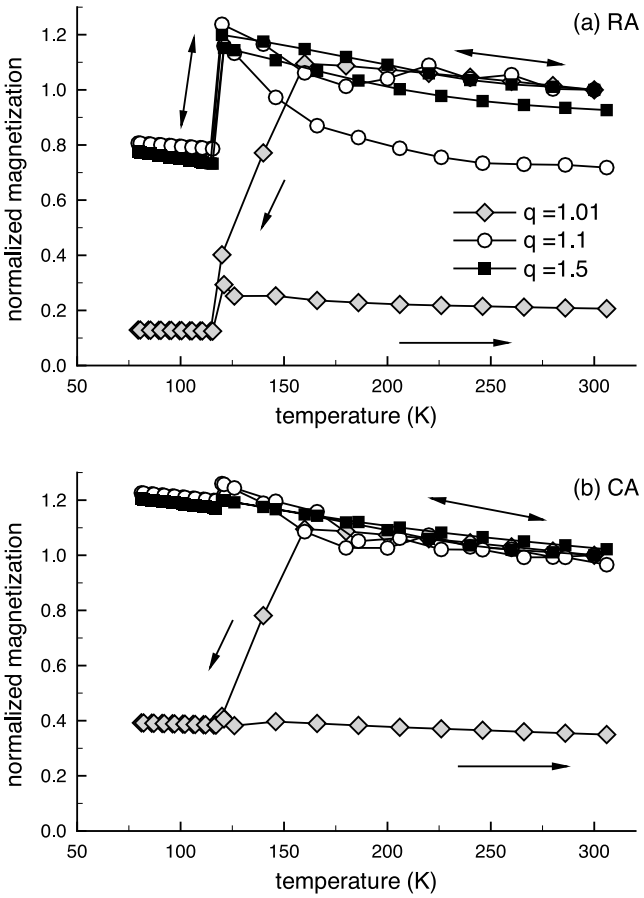

Figure 5. Simulated SIRM LTC curves for (a) the RA model and (b) the CA model for assemblages of randomly orientated noninteracting SD grains with various effective elongations. The uniaxial anisotropy is chosen randomly compared to the crystal morphology. Above T_V the samples have a cubic magnetocrystalline anisotropy; below T_V the samples have the monoclinic magnetocrystalline anisotropy. The symbols correspond to the simulated temperature steps.

elongation ratio q of the grain. The value of K_U is determined by using the standard formula $K_U = \mu_0 M_S^2 N(q)/2$, where μ_0 is the permeability of free space and $N(q)$ is the demagnetizing factor which is simply a function of q [*Nagata*, 1961]. $N(q)$ is positive; therefore E_A is minimized by the magnetization aligning with the elongation axis. M_S was taken to vary as $(1 - T/T_C)^{0.43}$, where T is temperature and T_C is the Curie temperature [*Dunlop and Özdemir*, 1997]. The value for the exchange constant was taken from *Heider and Williams* [1988] and was not varied with temperature.

[14] We modeled three-dimensional arrays of $10\times10\times10$ SD cubic grains distributed evenly, with randomly orientated anisotropies. Distributions of only 1000 grains have been shown to represent the behavior of larger arrays of randomly orientated distributions [*Muxworthy et al.*, 2004]. In the arrays the faces of the cubes are parallel to each other. We consider the effect of variations in magnetostatic interaction spacing (d/r), where d/r is the ratio of the grain size divided by the separation measured from the grain center, e.g., for touching grains d/r = 1, and as grains become further apart d/r $\rightarrow$ 0.

[15] For the highly interacting models there are small differences between repeat simulations, e.g., for the CA and RA cooling curves above the Verwey transition. For the highly interacting models the entire assemblage behaves effectively as one system. This system experiences a wide range of possible states on simulated cooling. On repeating the simulation occasionally different magnetic states are found. Simply increasing the assemblage size for the most interacting systems would not solve the problem.

[16] *Carter-Stiglitz et al.* [2002, 2004] modeled LTC curves for chains of interacting SD magnetite grains, i.e., an approximation to magnetosome chains found in magnetostatic bacteria. The effect of one-dimensional interactions has been shown to be different to that of interactions in two or three dimensions [*Muxworthy and Williams*, 2004]; they make magnetic assemblages behave more SD-like than MD-like. In this study we consider three-dimensional interaction fields.

3.2. Incorporation of Controlled Alignment Hypothesis

[17] On simulated low-temperature cycling for SD magnetite, we consider both a random alignment model (RA) of the monoclinic axes and a controlled alignment model (CA) as discussed in section 2. For the CA model, in addition to choosing the *c* axis closest to the direction of the magnetic moment of each grain, we also align the anisotropy within the *c* plane, i.e., in addition to controlling the orientation of the *c* axis, we also orientate the *a* axis (hardest direction) and the *b* axis (intermediate direction) in the *c* plane (Figures 1 and 4c). Because of symmetry there are only six possible orientations of monoclinic axis with respect to the cubic axis. On cooling through T_V, all three axes are orientated with respect to the magnetic moment, i.e., there is no random choice of axis orientation as in the RA model.

[18] We make the assumption that no crystallographic twins form within the SD grains. This is based on two considerations: first, the smallest reported low-temperature twin-domain structures are >20 μm [*Medrano et al.*, 1999], and second, if the boundary conditions were sufficient to cause twin structures to form in SD grains, i.e., <0.1 μm, it is unlikely that the magnetization would control the orientation of the monoclinic phase. The magnetic behavior of the sample shown in Figure 3 is unlikely to have been influenced by its boundary conditions, as it was embedded in CaF_2 giving it effectively a free surface.

4. Random Morphology

4.1. Noninteracting SD Assemblages

[19] Initially, we compare the predicted behavior of the RA and CA models with the calculations of *Carter-Stiglitz et al.* [2004]. We model assemblages of noninteracting, identical SD grains. Both uniaxial and cubic anisotropy are included, where the two anisotropies are randomly orientated with respect to both the field and each other, i.e., the effective elongation is chosen randomly with respect to the crystal morphology. Three different values of q are considered; q = 1.01 (cubic magnetocrystalline dominates at room temperature), q = 1.1 (cubic magnetocrystalline is twice that of the uniaxial anisotropy at room temperature) and q = 1.5 (uniaxial anisotropy dominates at room temperature). A value of q = 1.01 was chosen over q =

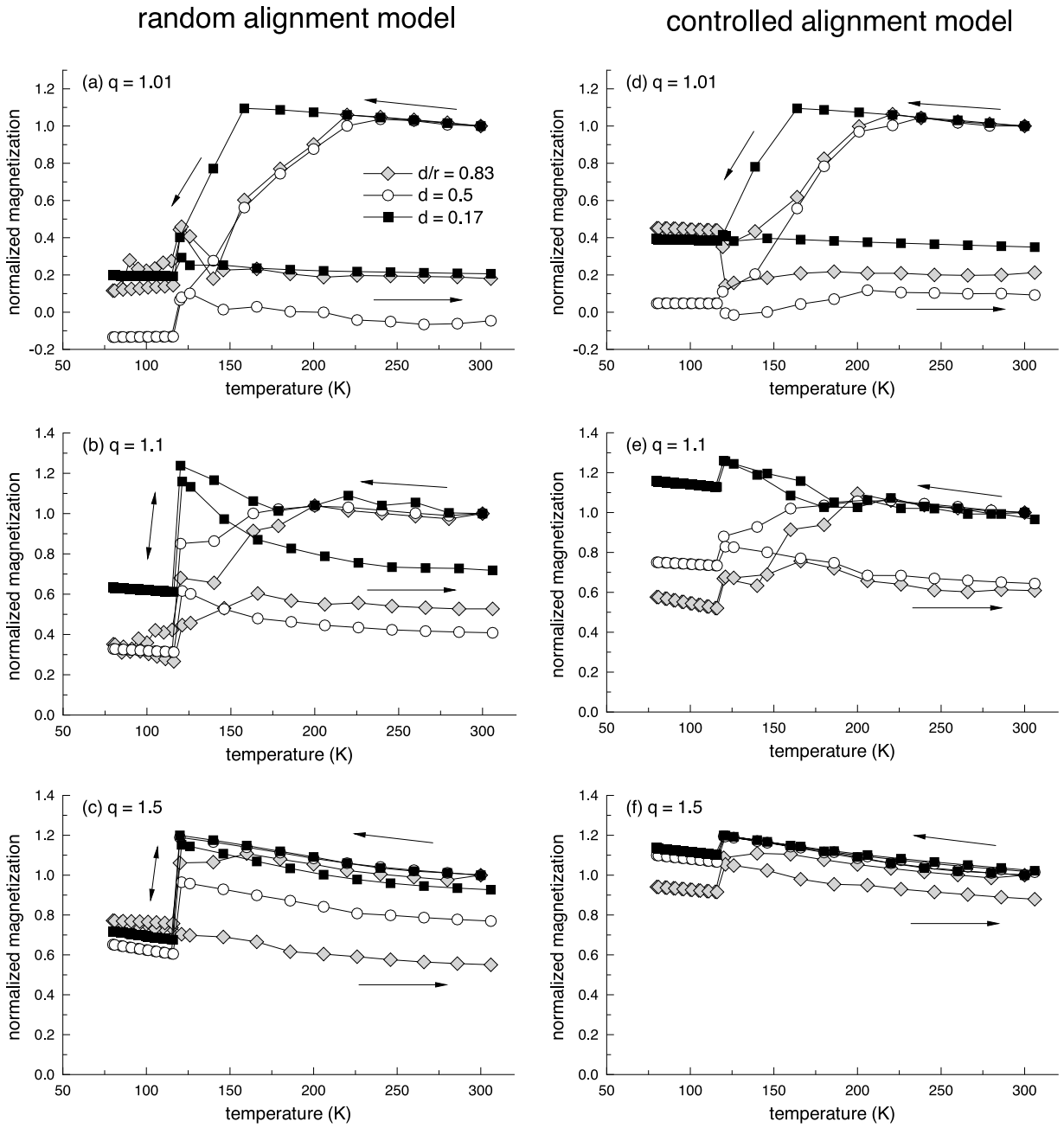

Figure 6. Simulated SIRM LTC curves for assemblages of randomly orientated SD grains with three effective elongations, i.e., q = 1.01, 1.1 and 1.5, and three magnetostatic interaction spacings. As d/r increases the spacing between grains decreases. (a)–(c) The RA model and (d)–(f) the CA model. The uniaxial anisotropy is chosen randomly compared to the crystal morphology.

1.0, for two reasons. First, because of the absence of thermal fluctuations in the model as the cubic anisotropy passes through an isotropic point at ~130 K [*Bickford et al.*, 1957], in the absence of the small uniaxial anisotropy and intergrain magnetostatic interactions, the SD moments will not rotate even though there is no energy barrier preventing them. Second, it is highly unlikely in reality that grains will have neither a small shape nor a stress-induced anisotropy, i.e., it is unlikely that an SD grain will be truly magnetically isotropic. For the three randomly orientated regimes, the initial SIRM/M_S ratios at 300 K were 0.86, 0.58 and 0.49 for q = 1.01, 1.1 and 1.5 respectively. For a randomly orientated assemblage, negative cubic anisotropy has an analytical SIRM/M_S value of 0.866, and uniaxial anisotropy that of 0.5 [*Kneller*, 1969]. Mixing cubic and uniaxial anisotropy changes these values, and for certain combinations SIRM/M_S < 0.5 [*Geshev et al.*, 1998]. The values calculated in this paper are in agreement with published numerical mixed-anisotropy calculations [*Geshev et al.*, 1998].

[20] For high values of q, the RA model SIRM LTC curves (Figure 5a) are identical to that predicted by *Carter-Stiglitz et al.* [2004] in Figure 2. On cooling to T_V the remanence signal increases as M_S increases. The LTC curve for q = 1.5 displays a large reversible decrease in the

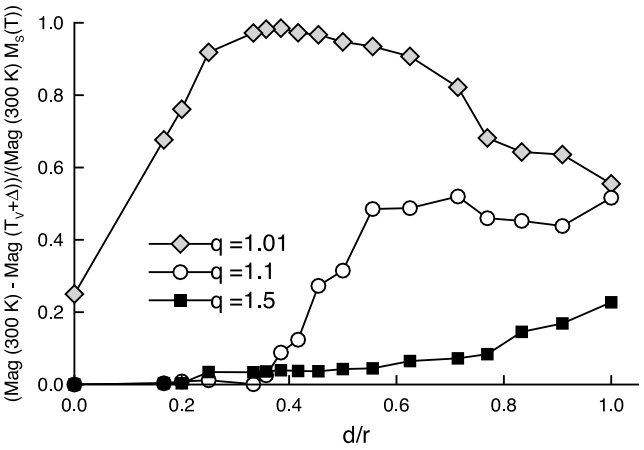

Figure 7. Quantification of the demagnetization on simulated cooling from 300 K to just above T_V. The demagnetization is normalized by the initial magnetization at 300 K, and the variation in M_S(T) is accommodated for. As the demagnetization occurs on cooling to above T_V, these curves are the same for both the RA and CA models. The uniaxial anisotropy is chosen randomly with respect to he crystal morphology.

magnetization at T_V, i.e., $\Delta_J < 0$, and the resulting memory ratio is slightly less than 1. This corresponds to the switching sequence shown through Figures 4a, 4b, and 4d. As q decreases, the influence of cubic magnetocrystalline anisotropy not included in the *Carter-Stiglitz et al.* [2004] calculations is seen. For q = 1.01, on simulated cooling to above T_V the remanence, which is controlled by the magnetocrystalline cubic anisotropy, demagnetizes as the cubic anisotropy decreases to zero at its isotropic point at ~130 K. On cooling through T_V the remanence displays a small decrease in demagnetization, i.e., small negative Δ_J. On increasing to 300 K, the curves are not reversible and MR < 1. This is similar to the behavior observed for MD material [*Muxworthy and McClelland*, 2000], and in contrast to Figure 2 where even as $q \rightarrow 1$, MR = 1. For q = 1.1, the LTC behavior falls between the other two cases, noticeably MR < 1.

[21] Results for the CA model are similar to the RA model (Figure 5), though for higher values of q, Δ_J is considerably reduced. This corresponds to the sequence shown in Figures 4a, 4c, and 4d; the starting and end states are the same, but due to the controlled switching mechanism at TV, Δ_J is relatively smaller as the c axis aligns with the closest ⟨100⟩axis. For q = 1.1 and 1.5, MR is close to 1. For q = 1.01, MR is larger compared to the RA model.

4.2. Effect of Magnetostatic Interactions

[22] The effect of varying the interaction spacing (d/r) between the grains is considered for the RA and CA models (Figure 6), where d/r is the ratio of the grain size divided by the separation measured from the grain center, e.g., for touching grains d/r = 1, and as grains become further apart d/r → 0. Certain key features are true for both the models; the degree of demagnetization increases on cooling between 300 K and to just above T_V, as d/r increases, i.e., increasing interactions (Figure 6). This demagnetization is quantified in Figure 7, by comparing the magnetization at 300 K with that just above T_V, allowing for the variation in M_S(T). For q = 1.01, the degree of demagnetization is highest for intermediate values of d/r, decreasing slightly as d/r → 1. Even for q = 1.5, the decrease in the cubic magnetocrystalline anisotropy on cooling is sufficient to cause a small degree of demagnetization, which increases with interactions (Figure 7). In addition for q = 1.5, as d/r increases, MR decreases (Figure 8). The influence of interactions is more pronounced in the RA model results than the CA simulations. For example, for q = 1.5 and d/r = 0.17, MR ~0.9 for the CA model, but 0.5 for the RA model (Figure 8). The reason for this is demonstrated in the schematic cartoon for possible switching sequences in the RA and CA models with the same initial starting state shown in Figure 9. On cooling through T_V, in the CA model the moment switches to the closest ⟨100⟩ axis (Figure 9c), whereas in the RA model it switches to a former ⟨100⟩ axis which lies at a greater angle from the original SIRM field direction (Figure 9b). On warming up to room temperature, in the CA mode the moment returns approximately to its original position subject to variations in the interaction field (Figure 9e), whereas in the RA model, the moment reverses aligning with the uniaxial anisotropy in the other direction, leading to an effective demagnetization (Figure 9d).

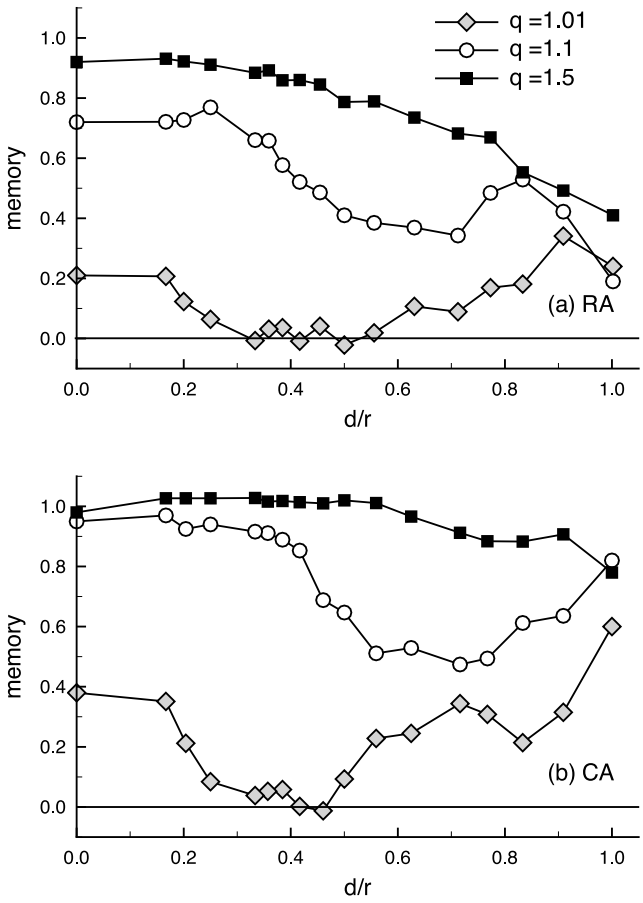

Figure 8. Magnetic memory ratio (MR) versus d/r for (a) the RA model and (b) the CA model for three effective elongations, i.e., q = 1.01, 1.1 and 1.5. As d/r increases the spacing between grains decreases. The uniaxial anisotropy is chosen randomly compared to the crystal morphology.

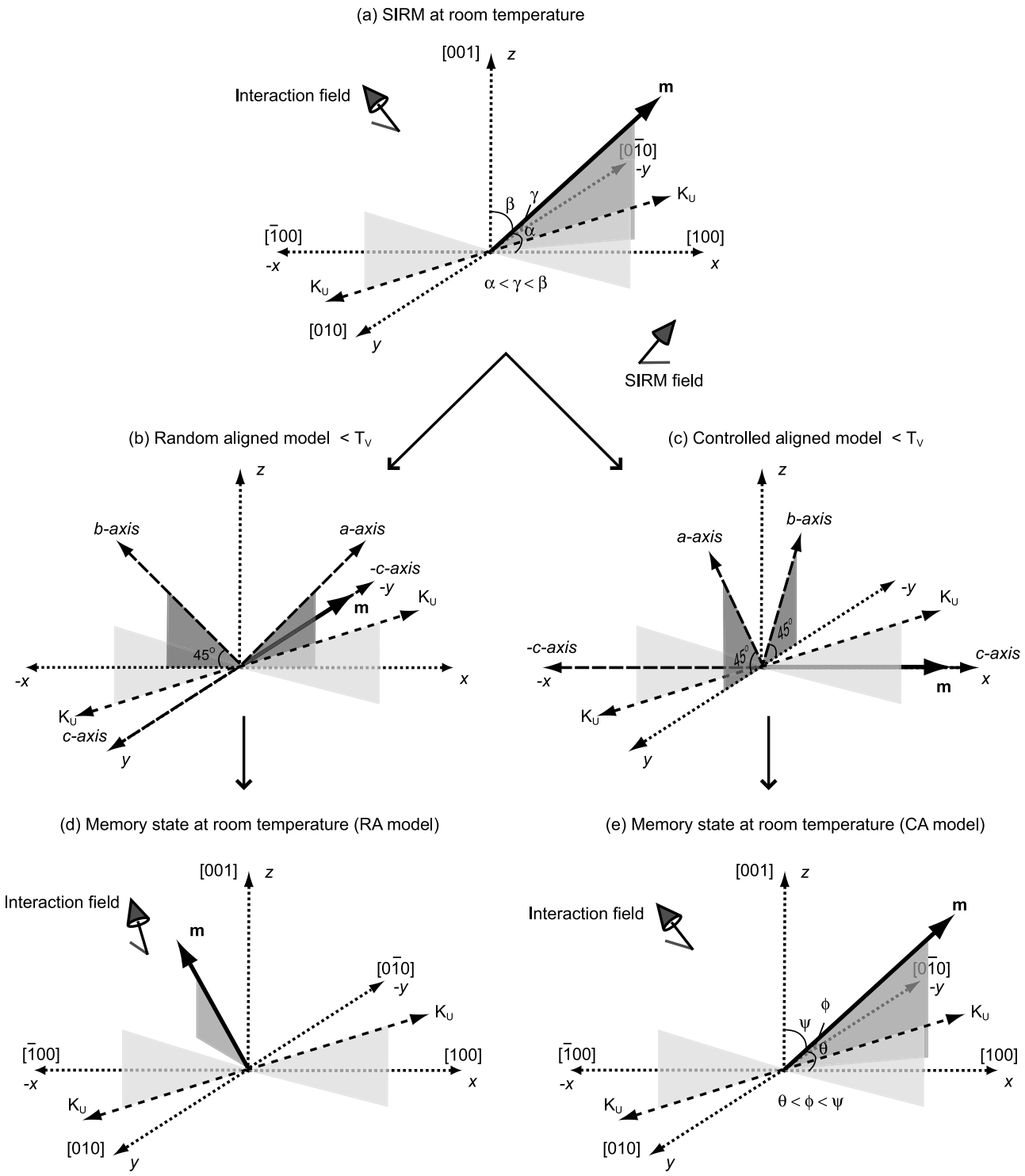

Figure 9. Schematic cartoon of the LTC SIRM behavior of a moment controlled by a uniaxial anisotropy at room temperature for both the RA and CA models in the presence of local magnetostatic interaction fields. From the same initial SIRM starting state (Figure 9a), the RA model switching behavior is shown in Figures 9b and 9d and for the CA model in Figures 9c and 9e. Because of the interaction field, the moment in Figure 9a does not align with the uniaxial anisotropy (K_U) but finds an equilibrium state dependent on the uniaxial anisotropy and the interaction field. In CA model the moment switches to the closest ⟨100⟩ on passing through T_V. In the RA model the *c* axis is randomly chosen. On warming back through T_V the moment in the RA model (Figure 9d) moves toward the closest K_U direction, which is in the opposite direction to Figure 9a and finds a new equilibrium position in the new interaction field. In the CA model the moment returns to approximately the same position as in Figure 9a subject to small variations in the interaction field.

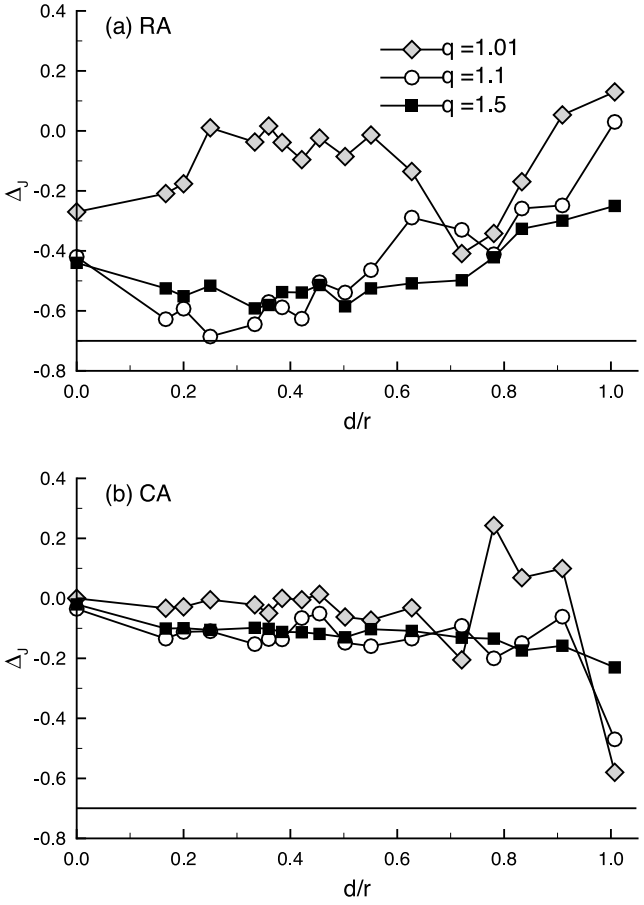

Figure 10. Δ_J versus d/r for (a) the RA model and (b) the CA model for three effective elongations, i.e., q = 1.01, 1.1, and 1.5. The uniaxial anisotropy is chosen randomly compared to the crystal morphology.

[23] The size and sign of Δ_J are strongly influenced by interactions (Figure 10). The model results for Δ_J become increasingly noisy as d/r is increased; this is likely due to the complex behavior of highly interacting systems. For the RA model for q = 1.1 and 1.5 and for small d/r, Δ_J is $\ll 0$, but increases as d/r $\rightarrow$ 1. In contrast, for the CA model, Δ_J for all three values of q, is generally > -0.2, except when d/r $\rightarrow$ 1 Δ_J displays greater variation.

5. Discussion

[24] The inclusion of the magnetocrystalline anisotropy and magnetostatic interactions in our RA model produces LTC behavior which is closer to the observed behavior than that predicted by *Carter-Stiglitz et al.* [2004]; in particular, the large negative Δ_J values (Figure 2) which are not observed experimentally are greatly reduced. However, there still appears to be some discrepancies between the RA model results and experimental results. Primarily, the model predicts significant demagnetization during LTC for equidimensional crystals, i.e., small q, which is not observed experimentally for SD near-cubic crystals (Figure 3). The effect of introducing the CA model is to increase MR for grains with small shape anisotropies (Figure 8). In addition, the CA model further reduces the large negative values of Δ_J compared to the RA model (Figure 10), suggesting that the CA model is a physically realistic mechanism for low-temperature monoclinic axis switching behavior. Positive Δ_J values observed experimentally are not found in the models except for large values of d/r, but simulated LTC curves with positive Δ_J values do not exhibit the same overall behavior as the experimental curves with positive Δ_J (Figures 3, 5, and 6), e.g., when d/r $\rightarrow$ 1 the LTC curves become less smooth and more erratic, in contrast to the experimental results.

[25] Both the CA and RA models in this paper for assemblages of randomly elongated SD grains predict behavior closer to the observed behavior than the simplified RA model of *Carter-Stiglitz et al.* [2004], and the CA model predicts behavior closer to that observed than the RA model. Yet even the CA model does not predict all the experimental behavior (Figure 3), i.e., reversible LTC curves with positive Δ_J and high memory ratios.

[26] In the initial simulations in this paper the uniaxial anisotropy was chosen randomly with respect to the cubic anisotropy. This assumption may be invalid for two reasons; first, there maybe a preferred direction of crystal growth, and secondly, by modeling only ideal single domain grains we have ignored the contribution of configurational anisotropy (W. Williams et al., Configurational anisotropy in single-domain and pseudo-single-domain grains of magnetite, submitted to Journal of Geophysical Research, 2006, hereinafter referred to as Williams et al., submitted manuscript, 2006). The configurational anisotropy is a term coined to describe the energy barrier associated with intermediate states in nonuniform SD or flower-state structures in symmetrical nonspherical grains, e.g., a cube, octahedron etc. For example, in a cubic grain with significant flowering it is energetically favorable for the magnetic structure to align with the axes of the cube, rather than through the corners. The energy associated with coherent rotation from one axis to another is the configurational anisotropy (W. Williams et al., submitted manuscript, 2006). Only a sphere will have no configurational anisotropy. Configurational anisotropy will always exist in cubic structures, but will often be masked by magnetocrystalline anisotropy or another anisotropy created by applied fields.

5.1. Nonrandom Orientations

[27] We now consider grains where the orientation of the shape/uniaxial anisotropy with respect to the crystal orientation is identical for each grain within the assemblage. We consider the two extreme cases, i.e., with the elongation in the $\langle 100 \rangle$ direction and the $\langle 111 \rangle$ direction. Numerical SIRM LTC simulations for q = 1.1 and 1.5 are shown in Figure 11 for both the RA and CA models. In Figures 12 and 13, MR and Δ_J are plotted as a function of d/r.

[28] In the RA model, for weakly interacting grains elongated along the $\langle 111 \rangle$ direction the LTC curves are reversible with large negative Δ_J values (Figures 11b and 11d). As the interactions increase the LTC curves becoming less reversible and MR decreases (Figure 12). In the RA model with grains elongated along the $\langle 100 \rangle$ direction, the LTC curves are nonreversible, with MR relatively independent of d/r (Figure 12) and large partially reversible negative-Δ_J behavior (Figures 11a, 11c, and 13).

[29] For weakly interacting grains elongated in the $\langle 111 \rangle$ direction with high values of q, the CA and RA models are

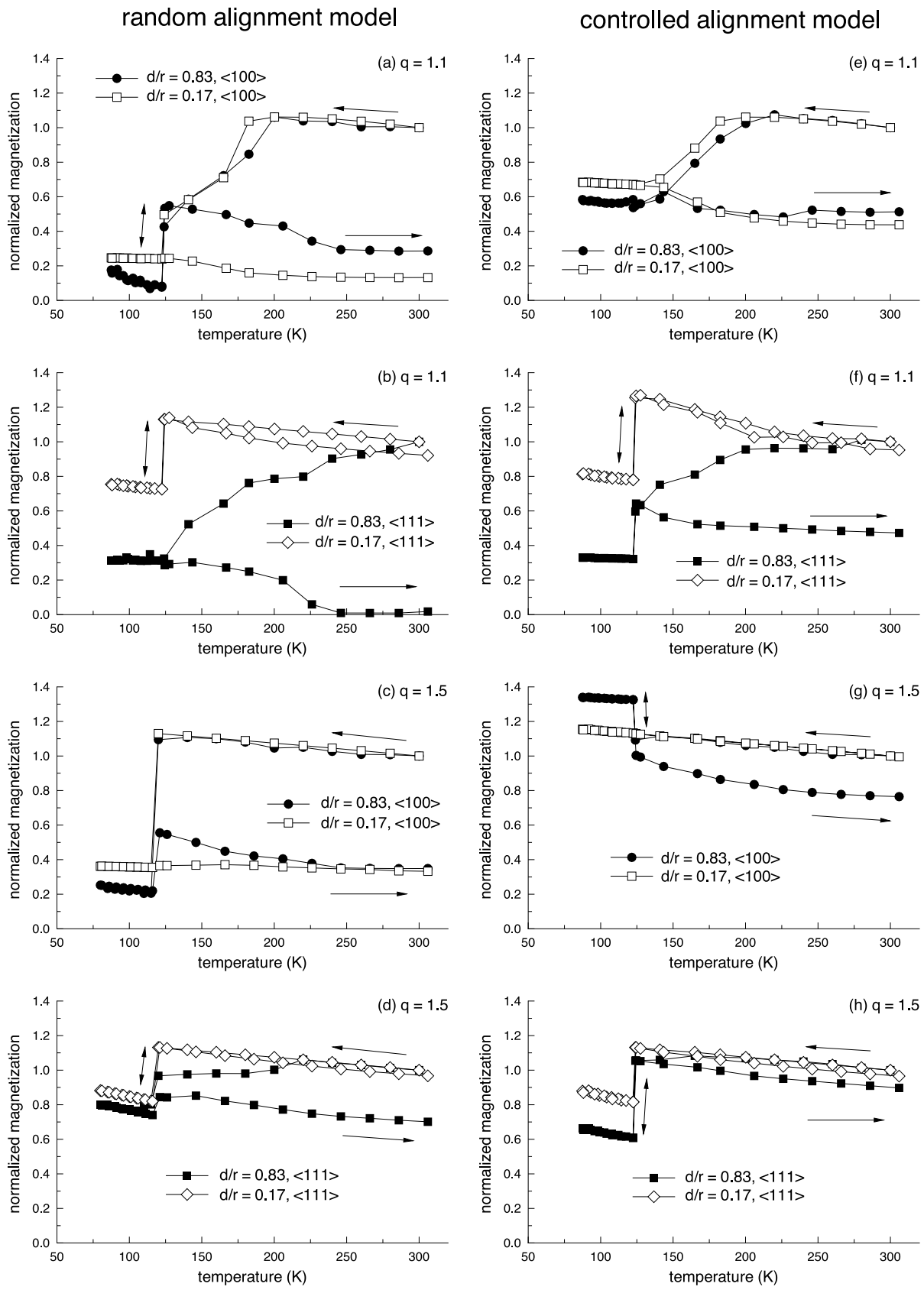

Figure 11. Simulated SIRM LTC curves for assemblages of nonrandomly orientated noninteracting SD grains with two effective elongations, i.e., q = 1.1 and 1.5, aligned along both (a), (c), (e) and (g) the $\langle 100 \rangle$ and (b), (d), (f) and (h) the $\langle 111 \rangle$ directions and two magnetostatic interaction spacings. Figures 11a–11d are for the RA model, and Figures 11e–11h for the CA model.

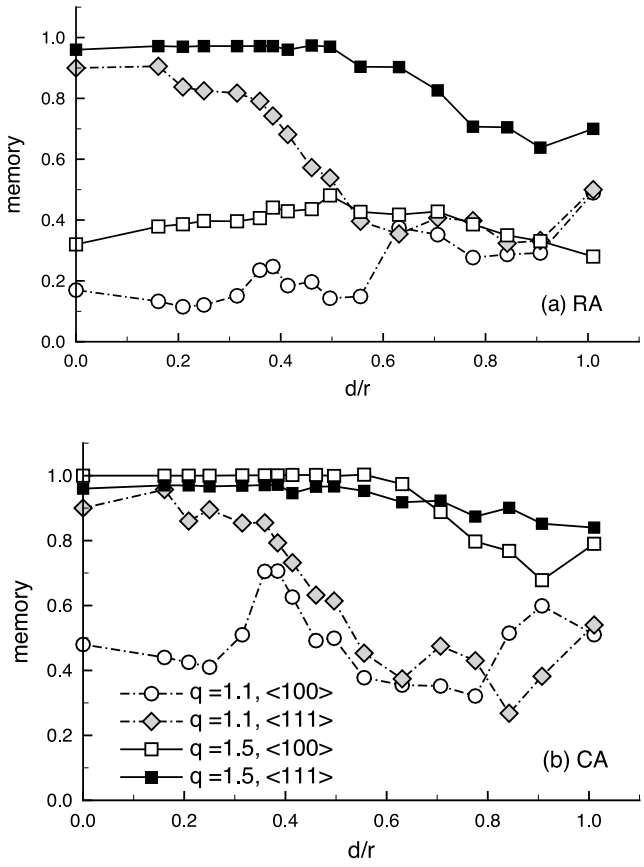

Figure 12. MR versus d/r for (a) the RA model and (b) the CA model for two effective elongations, i.e., $q = 1.1$ and 1.5 aligned along both the $\langle 100 \rangle$ and the $\langle 111 \rangle$ directions.

essentially the same. In the RA model, due to the relationship between the cubic and monoclinic crystallographic symmetries, the magnetic moment of each grain becomes "trapped" in one hemisphere of the uniaxial anisotropy ellipsoid, and the random choice of the low-temperature c axis in the RA model is the same as the CA model. The choice of the second axis will not be same, giving rise to the slight differences between the CA and RA models for $q = 1.1$ and 1.5 in Figures 11, 12, and 13. As d/r increases local magnetostatic interaction fields begin to dominate over the uniaxial anisotropy, and the similarity between the models breaks down. Δ_J is negative at all times in the $\langle 111 \rangle$ models.

[30] In contrast, for grains elongated along the $\langle 100 \rangle$ direction the difference in behavior between the CA and RA models is significant. The SIRM LTC curves become more reversible and MR is seen to increase for the CA compared to the RA model (Figures 11 and 12). On cooling though T_V $\Delta_J > 0$; for $q = 1.5$ Δ_J increases steadily from d/r = 0 to 0.91, it then decreases slightly for d/r = 1 (Figures 11g and 13). For $q = 1.1$, Δ_J peaks at d/r $\sim$ 0.7.

[31] On inducing an SIRM in these aligned assemblages of noninteracting grains elongated along the $\langle 100 \rangle$ axis, the moments of the grains will align along the elongated $\langle 100 \rangle$ axis at room temperature. As the degree of interactions increases, the grain moments deviate from the $\langle 100 \rangle$ axis. If the degree of interactions is significant then SIRM/M_S will be reduced. On cooling through T_V, if the degree of interactions is moderate, the moments rotate to the closest c axis, which for the CA model corresponds the elongated $\langle 100 \rangle$ axis/easy uniaxial axis. On average this will give rise to an increase in the magnetization. If, however, the degree of interactions is very large, then some moments will have rotated so far away from easy uniaxial anisotropy direction that the chosen c axis will not coincide with the uniaxial anisotropy, and the magnetization will decrease. This is why Δ_J decreases slightly as d/r $\rightarrow$ 1. This decrease with increasing d/r is more pronounced in the $q = 1.1$, $\langle 100 \rangle$ model as the uniaxial anisotropy field is weaker. This effect is not seen in the $\langle 111 \rangle$ models as the monoclinic easy axis, i.e., the c axis, does not correspond to an easy uniaxial anisotropy direction. Positive Δ_J behavior will exist for other orientations of elongation, becoming more pronounced as the direction of uniaxial anisotropy becomes closer to a $\langle 100 \rangle$ direction.

[32] Such positive Δ_J behavior has been predicted by models of multidomain LTC behavior [*Muxworthy and Williams*, 1999]. In these models it was found that the removal of closure-domain-like structures near the surface of the grain was the cause of the increase in magnetization on cooling through T_V. Highly interacting SD assemblages behave in many respects in a similar manner to MD assemblages, e.g., highly interacting SD assemblages have

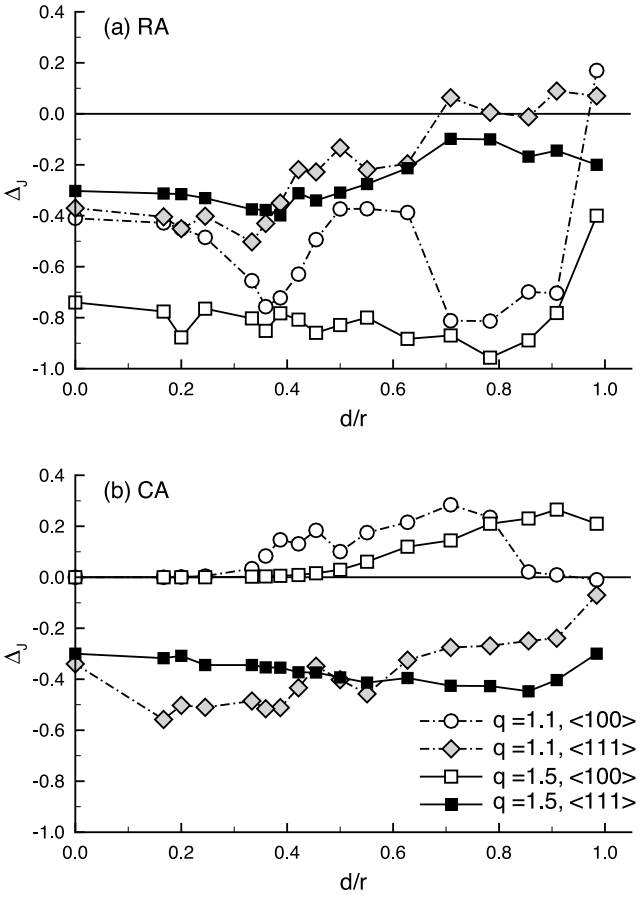

Figure 13. Δ_J versus d/r for (a) the RA model and (b) model for two effective elongations, i.e., $q = 1.1$ and 1.5 aligned along both the $\langle 100 \rangle$ and the $\langle 111 \rangle$ directions.

hysteresis parameters which are characteristic of MD grains [*Muxworthy et al.*, 2003b].

5.2. Comparison With Experimental Data

[33] Compared to the experimental data (Figure 3), the simulated SIRM LTC curves are less smooth and display more abrupt features, in particular at the Verwey transition temperature. The exact Verwey temperature for "perfect magnetite" is thought to be 125 K [*Walz*, 2002]; however, this temperature is easily suppressed by small deviations from stoichiometry and low levels of residual stress. In real samples each grain is likely to have a slightly different Verwey transition temperature leading to a distribution of transition temperatures ($\sim$120–125 K) in an assemblage of grains, "smoothing" the observed Verwey transition. In addition there are other differences between the model and the actual experimental samples, which will contribute to their LTC behavior; unlike the model, real samples will have distributions of grain spacing and coercivity. While these distributions can be included in the model, it is the purpose of the model to try to understand and interpret the main features of the experimental data; this is done by isolating key parameters.

[34] The positive Δ_J values in the near-cubic magnetite samples of *Özdemir et al.* [2002] (Figure 3), can be explained by the CA model with some magnetostatic interactions if the magnetization on average aligns with the $\langle 100 \rangle$ directions, either due to preferred direction of crystal elongation, configurational anisotropy or a combination of the two. That the grains are interacting is supported by the SIRM/M_S ratio which is $\sim$0.28 [*Özdemir et al.*, 2002]. For SD magnetite controlled by the cubic magnetocrystalline anisotropy alone, this indicates a spacing of d/r $\sim$ 0.45 [*Muxworthy et al.*, 2003b]. The SIRM LTC behavior and the relatively high MR for this SD sample (Figure 3), suggests that a uniaxial anisotropy dominates the behavior and the effective elongation q is > 1.3.

6. Conclusions

[35] The introduction of the cubic magnetocrystalline anisotropy and magnetostatic interactions to the model of *Carter-Stiglitz et al.* [2004] (Figure 2) is seen to significantly alter the LTC behavior (Figures 5, 6, and 10), producing nonreversible behavior, i.e., MR < 1, with partial demagnetization on cooling from room temperature to above T_V. The random alignment model of *Carter-Stiglitz et al.* [2004], does not accommodate all the experimentally observed features, in particular, increases in the magnetization on cooling through T_V, i.e., $\Delta_J > 0$. A new "controlled switching" model is developed, which predicts positive Δ_J behavior that the "random" model does not. In this model the orientation of the low-temperature monoclinic axes are not chosen randomly, but instead are controlled by the direction of the magnetic moment on cooling through the Verwey transition. Positive Δ_J behavior is only observed for grains with a uniaxial anisotropy aligned with or near to the $\langle 100 \rangle$ directions; uniaxial anisotropy aligned along the $\langle 111 \rangle$ axes produces negative Δ_J behavior. Thus for assemblages of SD magnetite whose LTC behavior is shown in Figure 3, this suggests that there is a preference for the magnetic moments to align along the $\langle 100 \rangle$ directions, i.e., the hard cubic magnetocrystalline anisotropy direction. This could be due to a preferred growth direction or configurational anisotropy (W. Williams et al., submitted manuscript, 2006).

[36] This proposed CA model is likely to only apply to grains of magnetite that have unconstrained surfaces free from stress. If the surfaces of a grain are not free, then it is likely that the monoclinic crystallographic axes will orientate in response to these boundary conditions, and not the internal magnetic structure of the grain. That is, only in stoichiometric magnetite will monoclinic axes orientation be controlled by the magnetic moment of the grain, and in nonstoichiometric magnetite the monoclinic axes will orientate in response to the stress fields within the grain. At no time will the monoclinic axes be chosen at random.

[37] The LTC curves for SD magnetite controlled by magnetocrystalline anisotropy (Figures 6a–6d) and/or subject to intergrain magnetostatic interactions (Figure 11), display LTC behavior more commonly associated with MD grains. Noninteracting SD magnetite grains dominated by cubic magnetocrystalline anisotropy can carry geologically stable remanences, however, if LTC curves were measured for such grains, then they would be incorrectly identified as MD grains which normally carry soft remanences. Therefore LTD procedures commonly used in paleointensity studies [e.g., *McClelland and Briden*, 1996; *Yamamoto and Tsunakawa*, 2005] can also remove stable SD remanences in addition to relatively unstable MD remanence.

[38] What are required now are a series of controlled experimental on well-characterized, stoichiometric SD magnetite grains with known or controlled interaction spacings, to test the models proposed in this studies.

[39] **Acknowledgment.** This work was funded through NERC research grant NE/C510159/1 to W.W. and A.R.M. and Royal Society funding to A.R.M.

References

Abe, K., Y. Miyamoto, and S. Chikazumi (1976), Magnetocrystalline anisotropy of low temperature phase of magnetite, *J. Phys. Soc. Jpn.*, *41*, 1894–1902.

Argyle, K. S., and D. J. Dunlop (1990), Low-temperature and high-temperature hysteresis of small multidomain magnetites (215–540 nm), *J. Geophys. Res.*, *95*, 7069–7083.

Bickford, L. R., J. M. Brownlow, and R. F. Penoyer (1957), Magnetocrystalline anisotropy in cobalt-substituted magnetite single crystals, *Proc. Inst. Electr. Eng.*, *B104*, 238–244.

Brown, P. N., G. D. Byrne, and A. C. Hindmarsh (1989), VODE: A variable coefficient ODE solver, *SIAM J. Sci. Stat. Comput.*, *10*, 1038–1051.

Brown Jr., W. F. (1963), *Micromagnetics*, John Wiley, Hoboken, N. J.

Carter-Stiglitz, B., M. Jackson, and B. Moskowitz (2002), Low-temperature remanence in stable single domain magnetite, *Geophys. Res. Lett.*, *29*(7), 1129, doi:10.1029/2001GL014197.

Carter-Stiglitz, B., B. Moskowitz, and M. Jackson (2004), More on the low-temperature magnetism of stable single domain magnetite: Reversibility and non-stoichiometry, *Geophys. Res. Lett.*, *31*, L06606, doi:10.1029/2003GL019155.

Carvallo, C., and A. R. Muxworthy (2006), Low-temperature first-order reversal curve (FORC) diagrams for synthetic and natural samples, *Geochem. Geophys. Geosyst.*, doi:10.1029/2006GC001299, in press.

Dunlop, D. J., and Ö. Özdemir (1997), *Rock Magnetism: Fundamentals and Frontiers*, 573 pp., Cambridge Univ. Press, New York.

Geshev, J., A. D. C. Viegas, and J. E. Schmidt (1998), Negative remanent magnetization of fine particles with competing cubic and uniaxial anisotropies, *J. Appl. Phys.*, *84*, 1488–1492.

Heider, F., and W. Williams (1988), Note on temperature dependence of exchange constant in magnetite, *Geophys. Res. Lett.*, *15*, 184–187.

Kneller, E. (1969), Fine particle theory, in *Magnetism and Metallurgy*, edited by A. Berkowitz and E. Kneller, pp. 366–472, Elsevier, New York.

Kronmüller, H., R. Schützenauer, and F. Waltz (1974), Magnetic after-effects in magnetite, *Phys. Status Solidi A*, *24*, 487–494.

McClelland, E., and J. Briden (1996), An improved methodology for Thellier-type paleointensity determination in igneous rocks, and its usefulness for verifying primary thermoremanence, *J. Geophys. Res.*, *101*, 21,995–22,014.

Medrano, C., M. Schlenker, J. Baruchel, J. Espeso, and Y. Miyamoto (1999), Domains in the low-temperature phase of magnetite from synchrotron-radiation X-ray topographs, *Phys. Rev. B*, *59*, 1185–1195.

Muxworthy, A. R., and E. McClelland (2000), The causes of low-temperature demagnetization of remanence in multidomain magnetite, *Geophys. J. Int.*, *140*, 115–131.

Muxworthy, A. R., and W. Williams (1999), Micromagnetic models of pseudo-single domain grains of magnetite near the Verwey transition, *J. Geophys. Res.*, *104*, 29,203–29,217.

Muxworthy, A. R., and W. Williams (2004), Distribution anisotropy: The influence of magnetic interactions on the anisotropy of magnetic remanence, in *Magnetic Fabric: Methods and Applications*, edited by F. Martín-Hernández et al., *Geol. Soc. Spec. Publ.*, *238*, 37–47.

Muxworthy, A. R., and W. Williams (2005), Magnetostatic interaction fields in first-order-reversal-curve (FORC) diagrams, *J. Appl. Phys.*, *97*, 063905.

Muxworthy, A. R., D. J. Dunlop, and Ö. Özdemir (2003a), Low-temperature cycling of isothermal and anhysteretic remanence: Microcoercivity and magnetic memory, *Earth Planet. Sci. Lett.*, *205*, 173–184.

Muxworthy, A., W. Williams, and D. Virdee (2003b), Effect of magnetostatic interactions on the hysteresis parameters of single-domain and pseudo-single-domain grains, *J. Geophys. Res.*, *108*(B11), 2517, doi:10.1029/2003JB002588.

Muxworthy, A. R., D. Heslop, and W. Williams (2004), Influence of magnetostatic interactions on first-order-reversal-curve (FORC) diagrams: A micromagnetic approach, *Geophys. J. Int.*, *158*, 888–897.

Nagata, T. (1961), *Rock Magnetism*, 2nd ed., 350 pp., Maruzen, Tokyo.

Nagata, T., K. Kobayashi, and M. D. Fuller (1964), Identification of magnetite and hematite in rocks by magnetic observations at low temperature, *J. Geophys. Res.*, *69*, 2111–2120.

Özdemir, Ö., and D. J. Dunlop (1999), Low-temperature properties of a single crystal of magnetite orientated along principal magnetic axes, *Earth Planet. Sci. Lett.*, *165*, 229–239.

Özdemir, Ö., D. J. Dunlop, and B. M. Moskowitz (2002), Changes in remanence, coercivity and domain state at low temperature in magnetite, *Earth Planet. Sci. Lett.*, *194*, 343–358.

Suess, D., V. Tsiantos, T. Schrefl, J. Fidler, W. Scholz, H. Forster, R. Dittrich, and J. Miles (2002), Time resolved micromagnetics using a preconditioned time integration method, *J. Magn. Magn. Mater.*, *248*, 298–311.

Walz, F. (2002), The Verwey transition: A topical review, *J. Phys. Condens. Matter*, *14*, R285–R340.

Williams, W., and D. J. Dunlop (1989), Three-dimensional micromagnetic modelling of ferromagnetic domain structure, *Nature*, *337*, 634–637.

Yamamoto, Y., and H. Tsunakawa (2005), Geomagnetic field intensity during the last 5 Myr: LTD-DHT Shaw palaeointensities from volcanic rocks of the Society Islands, French Polynesia, *Geophys. J. Int.*, *162*, 79–114.

A. R. Muxworthy, Institute of Earth Science, University of Edinburgh, Kings Buildings, West Mains Road, Edinburgh EH9 3JW, UK. (adrian.muxworthy@gmail.com)

W. Williams, Department of Earth Science and Engineering, South Kensington Campus, Imperial College, London SW7 2AZ, UK.